Studies of Dust Properties in Sub-Structures around White Dwarf WD 0307+077 in IRIS Survey

M. S. Paudel

Journal of Nepal Physical Society
Volume 8, No 1, 2022
(Special Issue: ICFP 2022)
ISSN: 2392-473X (Print), 2738-9537 (Online)

JNPS, **8** (1), 39-47 (2022)
DOI: http://doi.org/10.3126/jnphyssoc.v8i1.48284

Published by: Nepal Physical Society
P.O. Box: 2934
Tri-Chandra Campus
Kathmandu, Nepal
Email: nps.editor@gmail.com

ICFP 2022
ISSN:2392-473X (Print)
2738-9537 (Online)

Research Article ©Nepal Physical Society
DOI:http://doi.org/10.3126/jnphyssoc.v8i1.48284

Studies of Dust Properties in Sub−Structures around White Dwarf WD 0307+077 in IRIS Survey

M. S. Paudel[a)]

Department of Physics, Tri-Chandra Multiple Campus, Tribhuvan University, Kathmandu, Nepal

[a)]*mspaudel27@gmail.com, madhu.paudel@trc.tu.edu.np*

Abstract. A huge dust structure of size $3^\circ \times 3^\circ$ consisting of many sub−structures of dust nebulae and dust cavities is discovered around the WD 0307+077, located at RA (ICRS): 47.59°, DEC (ICRS): +7.84°, in far−infrared image of IRIS survey. Infrared flux density at 60 μm and 100 μm are used to calculate dust color temperature and dust mass in dust structure and all sub−structures. The contour plot is used to visualize the variation of infrared flux, dust color temperature and dust mass within all sub−structures. The inclination angle of isolated region of sub−structures is calculated to know the shape of the dust cloud. It is found that the dust color temperature of all the nebulae and cavities lies between the 20 K to 24 K, with range not more than 3 K. This range of temperature suggests that the sub−structures are moving towards the thermal stability. The dust mass shows the similar mass composition within all sub−structures, with variation of just one order magnitude. The linear regression shows a very good linear relation between between the infrared flux at 60 μm and 100 μm wavelength with regression coefficient more than 0.90 in five sub−structures and more than 0.78 in remaining two. The inclination angle of shows the all sub−structures are clearly *edge−on* in shape having inclination angle $i > 45^\circ$. The Gaussian distribution of dust color temperature in all sub−structures shows more or less deviation from Normal distribution, the background sources observed in the SIMBAD database are suspected for this deviation.

Received: 12 March, 2022; **Revised**: 16 April, 2022; **Accepted**: 8 May, 2022

Keywords: Dust Structure and Sub−structures; WD 0307+077; IRIS; Dust Color Temperature

INTRODUCTION

Study of interstellar dust enables us to explore the distribution of temperature and related phenomenon around the region. There have been many works exploring the properties of the dust within the nebulae [1], FIR loops [2, 3] Pulsar [4], Supernova remnants [5], White Dwarf [5] and many more. Study of dust cavity nearby the Pulsar at Galactic latitude: -60° shows the variation of dust color temperature from 22.78 K to 24.78 K and concluded that the cavity structure is less disturbed from nearby Pulsar and it's radiation [4]. The study of FIR loop (cavity) at Galactic latitude: -5° near the Pulsar J1627−5547 shows temperature variation of 16 K suggesting the cavity is dynamically active, which consist of a more stable core region having temperature variation less than 3 K [2]. In the study of dust properties within a dust structure located at Galactic latitude 0.04° nearby Supernova remnants G053.41+00.3, G053.9+00.2 and G053.1+00.3, a large fluctuation of dust color temperature more than 10 K is found [6]. It is reported that the dust structure is not in thermal equilibrium and the high energetic radiation sources observed in background are responsible for the large variation in temperature. A study of dust cavity nearby the White Dwarf WD 352−249 shows the variation of temperature 2.22 K suggesting the dust are evolving independently and less disturbed from the background radiation source [5].

There are large number of White Dwarf found in Milky Way around which prominent emission and condensation of dust is observed in far infrared data and many are not studied yet. In this work, dust structure around the White Dwarf WD 0307+077 selected. In 60 μm and 100 μm far infrared image of Improved Reprocessing of the IRAS Survey (IRIS) this dust structure is observed isolated from nearby regions. Furthermore, it is fragmented into many small isolated sub−structures. In this work the dust color temperature and dust mass is calculated within

the dust structure and sub−structures using the infrared flux density and presented the analysis of the result.

SOURCES OF DATA

In this research, the data from three public sources are used. The IRIS [7] data at 60 μm and 100 μm are the major data used for entire work. The FITS images in both wavelength of IRIS survey are downloaded from SkyView Virtual Observatory (`https://skyview.gsfc.nasa.gov`). The Gaia Early Data Release 3 (Gaia EDR3) are used from Gaia Archive (`https://gea.esac.esa.int/archive`) for the estimation of distance to the dust structure and sub−structures. The SIMBAD (`http://simbad.u-strasbg.fr/simbad/sim-fcoo`) data are used to study the background sources embedded within the dust structure.

METHOD

Dust Color Temperature and Dust Mass

The interstellar dust absorbs the radiation from the nearby sources and re−radiates the absorbed energy in the form of thermal radiation which belongs to the infrared band of electromagnetic radiation. The concept of blackbody emission can be used to estimate the dust color temperature following the method given by Wood *et al*. (1994) [8] and Schnee *et al*. (2005) [9]. The final expression of dust color temperature is given as;

$$T_d = \frac{-96}{ln\{R \times 0.6^{(3+\beta)}\}} \quad (1)$$

Where, R is the ratio of flux density at 60 μm and 100 μm and β is the spectral emissivity index which takes the values from 0 to 2 [10]. The longer wavelength can give the precious measurement of mass of the dust particles [9]. Therefore, the 100 μm image is used for the measurement of dust mass following the method of Young *et al*. (1993) [11] and Hildebrand (1983) [12]. The expression for calculation of mass of dust is;

$$M_{dust} = 0.4[\frac{S_\nu D^2}{B(\nu, T_d)}] \quad (2)$$

Where, S_ν is the flux density in SI unit = f $\times$ MJy/Str $\times$ 5.288 $\times$ 10^{-9}, 1 MJy/Str = 1 $\times 10^{-20}$ kg s^{-2}, f is the flux density, D is the distance to the dust structure and B(ν, T_d) is the Planck's function.

To calculate the mass of gas, we assume that the mass of gas is 200 times of the mass of the dust on the basis of Hildebrand (1983) [12].

Inclination Angle

The inclination angle (i) is the representation of the visual angle which can be defined as the angle made by the direction of visualization to the normal of the plane of the structure. The Holmberg (1946) [13] formula enables us for the calculation of inclination angle, which is given as;

$$cos^2 i = \frac{(\frac{b}{a})^2 - q*^2}{1 - q*^2} \quad (3)$$

Where, $\frac{b}{a}$ is the ratio of minor to major axis and $q*$ is the intrinsic flatness of the structure. In this work, the value of intrinsic flatness q* is taken 0.23 [14] assuming that the dust structure is oblate spheroidal in shape. The inclination angle decides whether the dust structure is edge−on, having value close to 90° or face−on, having value close to 0°.

RESULTS & DISCUSSION

Dust Structure and Sub−structures

A dust structure of size 3°×3° centered at RA (ICRS): 47.59°, DEC (ICRS): +07.84° is discovered around the White Dwarf WD 0307+077 in IRIS data. This White Dwarf is also recognized by the name HS 0307+0746. In the color map of infrared flux at 100 μm wavelength it is clearly seen that the dust structure consists of many isolated dust nebulae and dust cavities. The five nebulae are named as; N1, N2, N3, N4 and N5, here the letter N is used to represent the nebula, and the two cavities are represented by C1 and C2, C representing the cavity. The **FIGURE 1** shows the color map of dust structure for flux density at 100 μm in which five nebulae and two cavities are encircled by the rectangles. There are many White Dwarf and White Dwarf candidates within the dust structures, the WD 0307+077 is shown at the center of structure within N3. The other five White Dwarf are; SDSS J031224.51+064218.3, SDSS J030938.17+062414.1, SDSS J031238.28+062639.0, SDSS J031316.04+063102.2 and SDSS J031452.10+063238.4 all lying in the lower part of the dust structure.

In this paper, the all nebulae and cavities are called sub−structures. The **TABLE I** presents the many information of sub−structures, such as; the geometrical center, physical centers with maximum flux (for nebulae) and minimum flux (for cavity), isocontour level for in 100 μm FITS image in Aladin v2.5 and the average value of flux at this isocontour level.

TABLE I. The table shows the various information related to the center and size of all sub−structures.

Structure	Geometrical Center RA, DEC.	Physical Center RA, DEC.	Size	No. of Pixels	Isocontour Level	Flux at 100 μm MJy/sr
N1	48.23°, +08.56°	48.25°, +08.73°	0.55° × 0.55°	484	119	15.08 ± 0.04
N2	47.67°, +08.48°	47.64°, +08.44°	0.8° × 0.8°	1024	140	15.96 ± 0.03
N3	47.47°, +08.04°	47.37°, +08.10°	0.65° × 0.65°	676	121	15.98 ± 0.02
N4	46.82°, +07.46°	46.99°, +07.50°	1.20° × 1.20°	2304	159	15.49 ± 0.03
N5	48.15°, +07.06°	48.53°, +06.88°	1.60° × 1.60°	4096	134	14.60 ± 0.03
C1	48.58°, +07.87°	48.50°, +07.76°	0.6° × 0.6°	576	87	11.64 ± 0.02
C2	48.06°, +07.86°	48.02°, +07.88°	0.5° × 0.5°	400	93	10.53 ± 0.03

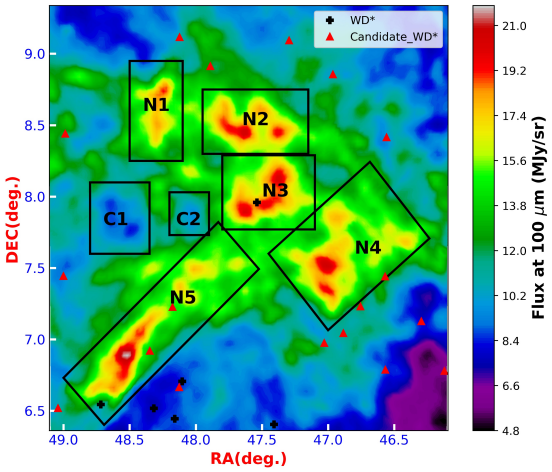

FIGURE 1. Figure shows the 3°×3° IRIS 100 μm FITS image of dust structure located (RA, DEC) (ICRS): (47.59°, +07.84°). The sub−structures are encircled by rectangles. Many White Dwarf and White Dwarf candidates are embedded within the dust structure, WD 0303+077 lies within N3.

Infrared Flux Density

The infrared flux density at two wavelengths, 60 μm and 100 μm are extracted from each pixels of the Flexible Image Transport System (FITS). For the extraction of the infrared flux Aladin v11.0 [15] is used. The size and the number of pixels of the each sub−structures is presented in the **TABLE I**. Interestingly, the flux at isocontour level creating the isolated region in all dust nebulae is almost same with the exception in N5, however there is also small deviation. This is also followed for the dust cavities C1 and C2.

The statistical information of infrared flux at both wavelengths, 60 μm and 100 μm are presented in **TABLE II**. In all dust nebulae the maximum, minimum and mean values of the flux at both wavelengths are more or less constant. A similar features in the statistical data of flux is also observed in dust cavities also. These all results shows that the all sub−structures (nebulae and cavities) have similar types of infrared characteristics possibly due to the evolution from same source.

Dust Color Temperature

The ratio of infrared flux density at 60 μm and 100 μm are used to calculate the dust color temperature following the method of Wood *et al*.(1994) [8] and Schnee *et al*.(2005) [9]. The value of spectral emissivity index β is taken 2 for the crystalline dielectric characteristic of the interstellar dust as suggested by Dupac *et al*. (2003) [10]. The statistical data of dust color temperature in each sub−structure is presented in **TABLE III**. The dust color temperature of the isolated region in 100 μm infrared flux is calculated separately. Interestingly, for N1 the maximum and minimum temperature both lies inside the isolated region and for N3, N4 and C2 the both maximum and minimum temperature lies outside the isolated region. For N2 and N5 maximum temperature lies inside and minimum temperature lies outside the isolated region. In C1 the maximum temperature lies outside and minimum temperature lies inside the isolated region. The contour map of temperature also explores this facts visually, which is discussed in later section. The average temperature of the isolated region increases for all sub−structures except C2 for which it is decreasing. The range of the temperature decreases for isolated region in comparison to the total region in all sub−structures, including all nebulae and cavities. Which is an obvious result. Furthermore, the range of temperature in all sub−structures is less than 3 K. This result suggest that the dust within all the sub−structures is moving towards the thermal stability.

TABLE II. Statistical information of infrared flux at 60 μm and 100 μm in dust structure and all sub−structures.

Structure	λ (μm)	F_{max} (MJy/sr)	F_{min} (MJy/sr)	F_{mean} (MJy/sr)	Range (MJy/sr)	SD (MJy/sr)	SE (MJy/sr)
Large	60	4.33	0.61	1.90	3.72	0.59	0.01
	100	21.74	4.84	11.79	16.92	2.82	0.02
N1	60	3.37	1.50	2.37	1.87	0.36	0.02
	100	19.28	11.03	14.67	8.25	1.69	0.08
N2	60	3.56	1.50	2.44	2.06	0.49	0.02
N2	100	20.37	10.54	14.76	9.83	2.20	0.07
N3	60	3.52	1.73	2.78	1.78	0.37	0.01
N3	100	20.30	11.92	15.82	8.38	1.83	0.07
N4	60	3.80	0.62	2.20	3.18	0.55	0.01
N4	100	20.78	5.14	13.22	15.64	2.84	0.05
N5	60	4.33	0.83	2.06	3.50	0.59	0.01
N5	100	21.74	6.31	11.91	15.43	2.75	0.04
C1	60	2.25	1.32	1.79	1.23	0.25	0.01
C1	100	14.75	8.26	10.80	6.50	1.24	0.05
C2	60	2.69	1.49	2.07	1.20	0.28	0.01
C2	100	15.23	9.60	12.35	5.63	1.28	0.01

TABLE III. The table shows the statistical information of dust color temperature in all square region and isolated region of all sub−structures, SD represents the standard deviation and SE represents the standard error. In second column all represents the square regions of nebula and cavity and isolated represents the isolated region in 100 μm infrared flux.

Strecture	Region	T_{max} (K)	T_{min} (K)	T_{av} (K)	Range (K)	SD (K)	SE (K)
Large	All	24.45 ± 1.30	20.18 ± 0.83	21.84 ± 0.01	4.27 ± 1.07	0.54	0.01
N1	All	22.70 ± 0.40	21.05 ± 0.43	21.91 ± 0.02	1.65 ± 0.43	0.37	0.01
	Isolated	22.70 ± 0.34	21.05 ± 0.49	22.02 ± 0.01	1.65 ± 0.41	0.41	0.01
N2	All	22.74 ± 0.37	21.03 ± 0.49	22.00 ± 0.01	1.71 ± 0.43	0.34	0.01
	Isolated	22.74 ± 0.22	21.85 ± 0.23	22.28 ± 0.01	0.89 ± 0.22	0.22	0.01
N3	All	22.73 ± 0.41	21.33 ± 0.29	22.15 ± 0.01	1.40 ± 0.35	0.20	0.01
	Isolated	22.51 ± 0.14	21.87 ± 0.18	22.23 ± 0.01	0.64 ± 0.16	0.13	0.01
N4	All	23.10 ± 0.54	20.32 ± 0.85	22.03 ± 0.01	2.79 ± 0.70	0.36	0.01
	Isolated	22.94 ± 0.32	21.64 ± 0.33	22.30 ± 0.01	1.30 ± 0.32	0.25	0.01
N5	All	23.28 ± 0.29	20.78 ± 0.41	22.22 ± 0.01	2.50 ± 0.35	0.35	0.01
	Isolated	23.28 ± 0.35	21.66 ± 0.46	22.59 ± 0.01	1.62 ± 0.41	0.28	0.01
C1	All	22.60 ± 0.27	21.38 ± 0.33	21.05 ± 0.01	1.22 ± 0.30	0.21	0.01
	Isolated	22.38 ± 0.23	21.38 ± 0.27	21.92 ± 0.01	0.99 ± 0.25	0.20	0.01
C2	All	22.75 ± 0.32	21.54 ± 0.28	22.11 ± 0.01	1.21 ± 0.30	0.26	0.01
	Isolated	22.55 ± 0.30	21.57 ± 0.19	21.94 ± 0.02	0.98 ± 0.24	0.19	0.02

Linear Relation between Infrared Fluxes

The far−infrared flux at 60 μm and 100 μm are used to calculate the dust color temperature. There might be some relation between them. The linear relationship between two infrared fluxes are checked using linear regression in Python 3.8. The slope of the straight line is used to calculate the dust color temperature. Assuming the slope as the average ratio R of two infrared flux, the average dust color temperature is calculated using equation (1). The best fitted straight line between infrared flux at 60 μm and 100 μm wavelength are shown in the **FIGURE 2**. The various parameters for best fit straight line are shown in **TABLE IV**. The r^2 value and graph both shows that there is strong linear relation between the two infrared fluxes as expected. The average temperature calculated using the slope of the best fit straight line are slightly deviated from

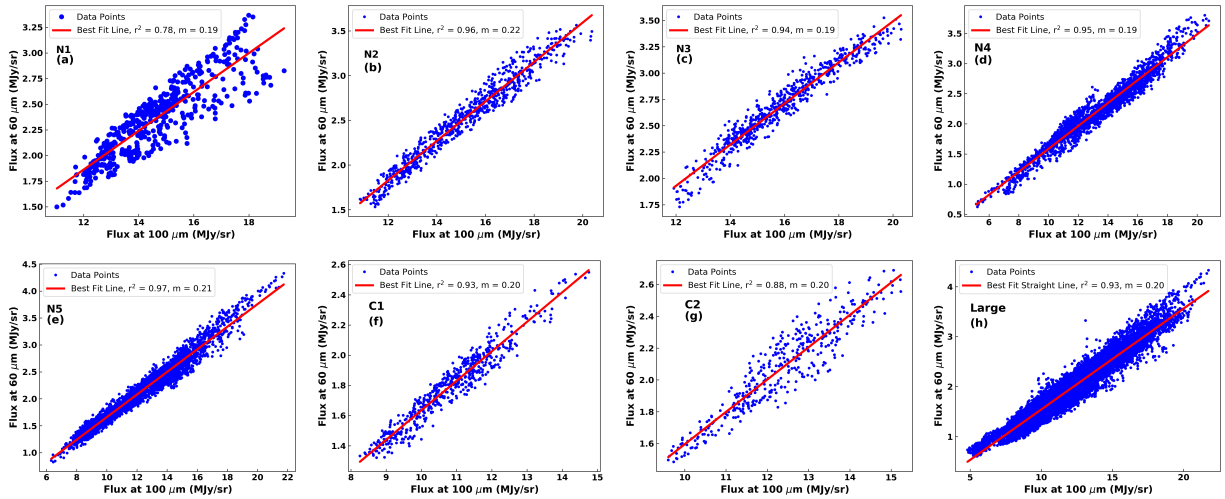

FIGURE 2. Figure shows the linear relation between two infrared fluxes in all sub−structures and large structure. The flux at 100 μm is taken along X−axis and flux at 60 μm is taking along Y−axis. Here, r^2 is the regression coefficient and m is slope of straight line.

TABLE IV. The table shows the parameters in linear fit, first column gives the name of structure and sub−structures, second column gives the equation of best fitted straight line, third column gives the regression coefficient and fourth column shows the average dust color temperature.

Structure	Best Fit Equation	r^2	T_d (K)
Large	$F(60) = 0.63F(100) - 0.48$	0.93	23.11
N1	$F(60) = 0.19F(100) - 0.41$	0.78	22.76
N2	$F(60) = 0.22F(100) - 0.82$	0.96	23.62
N3	$F(60) = 0.19F(100) - 0.42$	0.94	22.93
N4	$F(60) = 0.19F(100) - 0.32$	0.95	22.78
N5	$F(60) = 0.21F(100) - 0.44$	0.97	23.32
C1	$F(60) = 0.20F(100) - 0.32$	0.93	22.93
C5	$F(60) = 0.20F(100) - 0.44$	0.88	23.15

the average temperature of the total structure presented in **TABLE IV**. The difference in dust color temperature calculated from the slope of straight line might be due to the large value of y−intercept of the straight line.

Distance Estimation

The distance to the dust structure is calculated from parallax of the sources within the dust structure using Gala Early Third Data Release (Gaia EDR3) [16]. There are nearly 27,000 Gaia sources within the $3^\circ \times 3^\circ$ dust structure. Following sources are discarded; (i) having relative parallax error greater than 20 %, (ii) negative parallax, and (iii) parallax less than 40 mas and greater than 1 mas. After applying these criteria there are 6,167 objects remaining in data. The average parallax of these objects is 2.5045 mas. The average distance is calculated from the reciprocal of average parallax, which is 399.28 pc. This distance is used to calculate the dust mass in dust structure and all sub−structures.

Dust Mass

The mass of dust is calculated following the method of Young *et al*. (1993) [11] and Hildebrand (1984) [12], for which the value of flux density in SI unit, Planck's function and distance to the dust structure is required. The flux density in SI unit is calculated using the flux at 100 μm, Planck's function is calculate by using the dust color temperature at fixed wavelength 100 μm and distance of the all sub−structures is calculated using Gaia EDR3, which is 399.28 pc. The dust mass as well as the mass of gas within the all square region and isolated region is presented in the **TABLE V**. It is seen that the total mass of dust is in the order of 10^{28} kg in N1, C1 and C2 and in the order of 10^{29} kg in N2, N3, N4 and N5. This might be due to the fact that the size of the N1, C1 and C2 are smaller then N2, N3, N4 and N5. The mass of dust per pixels in all sub−structures is in the order of 10^{26} kg. The mass of dust in isolated region of all sub−structures is in the order of 10^{28} kg except N5, for which it is in the order of 10^{29} kg because it is quite larger in size. The variation trend of gas mass in sub−structures is similar to dust mass because it is obtained by multiplying the dust mass by 200.

TABLE V. Table presents the mass of Dust and Gas in kg and solar mass. First column gives the name structure and sub −structures, second and third columns gives dust mass and fourth and fifth columns gives the gas mass.

Structure	M_d (kg)	M_d ($M_\odot$)	M_g (kg)	M_g ($M_\odot$)
Large	1.98×10^{30}	1.00	3.96×10^{32}	199.22
N1: All	8.21×10^{28}	0.04	1.64×10^{31}	8.25
Isolated	3.00×10^{28}	0.02	6.00×10^{30}	3.02
N2: All	1.37×10^{29}	0.07	2.74×10^{31}	13.77
Isolated	4.53×10^{28}	0.02	9.05×10^{30}	4.55
N3: All	1.14×10^{29}	0.06	2.29×10^{31}	11.50
Isolated	4.95×10^{28}	0.02	9.89×10^{30}	4.97
N4: All	3.36×10^{29}	0.17	6.73×10^{31}	33.82
Isolated	6.65×10^{28}	0.03	1.33×10^{31}	6.68
N5: All	5.07×10^{29}	0.25	1.01×10^{32}	50.98
Isolated	1.10×10^{29}	0.06	2.21×10^{31}	11.10
C1: All	6.85×10^{28}	0.03	1.37×10^{31}	6.89
Isolated	2.32×10^{28}	0.01	4.64×10^{30}	2.33
C2: All	5.35×10^{28}	0.03	1.07×10^{31}	5.38
Isolated	1.27×10^{28}	6.41×10^{-3}	2.55×10^{30}	1.28

The total mass of the dust in isolated cavities C1 and C2 is quite low in comparison to the mass of dust in cavity nearby the WD 0359−249 studied by Paudel *et al*. (2021) [5], for which it is in the order of 10^{29} kg. This might be due to the small size of C1 and C2 compare to the cavity nearby WD 0359−249. However, the mass per pixels in all cavities are in the same order 10^{26} kg.

Contour Map: Infrared Flux, Dust Color Temperature and Dust Mass

The contour map with color plot enables us to distinguish the regions having different magnitude of the various parameter. The **FIGURE 3** shows the contour map with color plot for all sub−structures. There are four plots for each sub−substructures; first plot (a) for flux density at 60 μm, second plot (b) for flux density at 100 μm, third plot (c) for dust color temperature and fourth plot (d) for dust mass. For all sub−structures the contour plot for flux density at both wavelength looks similar however there is huge difference in the magnitude of flux density. The similar distribution is also manifested from the linear relation. From the contour map of dust color temperature and dust mass we can't infer any exact relation, the color distribution shows nonuniform variation between temperature and mass in all sub−structures. It can be suspected that the background sources are responsible for nonuniform variation of dust color temperature and dust mass among all sub−structures.

SIMBAD Background Source

SIMBAD enables us to know the objects within the dust structure. The all SIMBAD sources within the rectangular region of size $3^\circ\times3^\circ$ with center at (RA, DEC) (ICRS): (47.59°, +07.84°) are downloaded. There are 582 sources. The major sources are presented in **TABLE VI** and **FIGURE 4**. The many sources which are only one in numbers are absent in **TABLE VI**, such sources includes; BLLac, low-mass*, BYDra, PossibleCIG, AGN, RSCVin, Candidate-SN, GinGroup, SB*, RGB*, Seyfert, Candidate-HB*, Possible-GrG, C*, QSOCandidate, AGB* and gammaBurst. The name in OTYPE are given according to the SIMBAD.

TABLE VI. Major background sources taken from SIMBAD are presented below. OTYPE represents the types of source, name are given according the symbol used in SIMBAD and count represents their number. There are all together 582 sources within the selected rectangular region.

OTYPE	Count	OTYPE	Count
Star	190	WD*	6
Galaxy	67	**	6
PM*	62	Candidate-YSO	4
Radio	59	Possible-lensImage	3
FIR	22	AGN-Candidate	3
Candidate-WD*	18	ClG	3
X	17	IR	3
QSO	16	Cloud	2
MolCld	12	brounD*	2
RRLyr	12	GroupG	2
EB*	11	PairG	2
LensedImage	11	HI	2
HVCld	10	NIR	2
HB*	10	Pec*	2
V*	7	RGB*	1

Gaussian Distribution

The temperature of each pixels inside the isolated region of all sub−structures are modeled for Gaussian distribution as shown in **FIGURE 5**. The Gaussian distribution is more or less close to the Normal distribution. In N1, N3, N4 and C2 the distribution is slightly deviated and in N2, N5, C1 the distribution is very close to Normal distribution. There is no any significant difference in average temperature and range of temperature within these sub−structures, however it can be said that the external background sources that are observed in SIMBAD database are responsible for the deviation from Normal distribution.

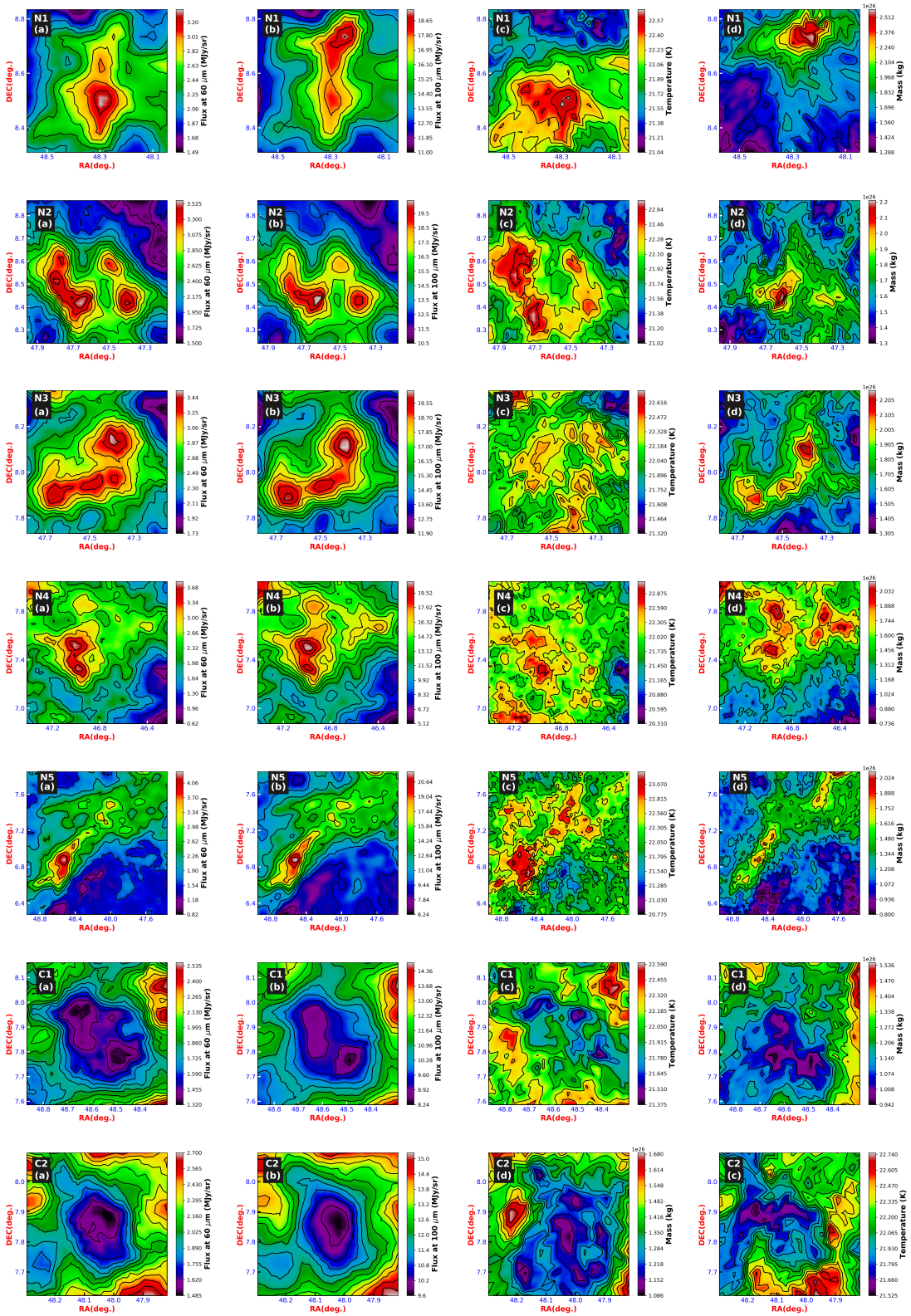

FIGURE 3. The contour maps for infrared fluxes (a and b), dust color temperature (c) and dust mass (d) for all sub−structures are shown in figure. The first row is for N1, second row for N2, third row for N3, fourth row for N4, fifth row for N5, sixth row for C1 and seventh row for C2.

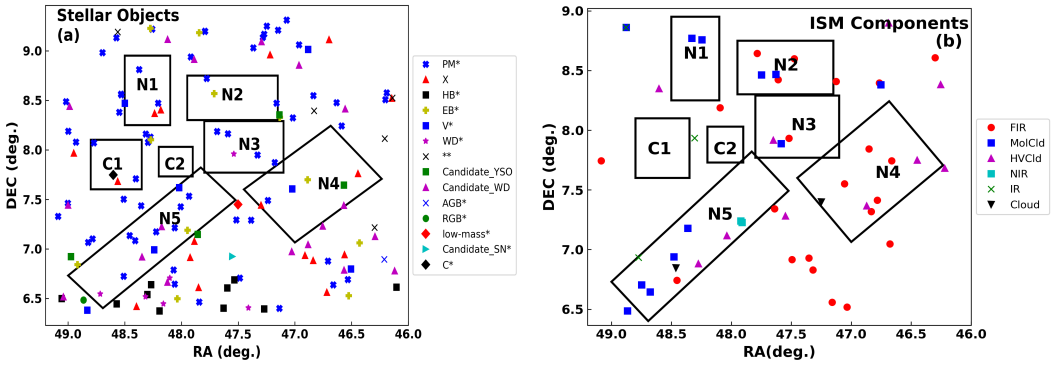

FIGURE 4. The figure shows the SIMBAD sources in the rectangular region of size $3^\circ \times 3^\circ$ and locations of all sub−structures. In all plot, RA is taken along X−axis, DEC is taken along Y−axis. Figure (a) for stellar objects and (b) for Interstellar Medium components.

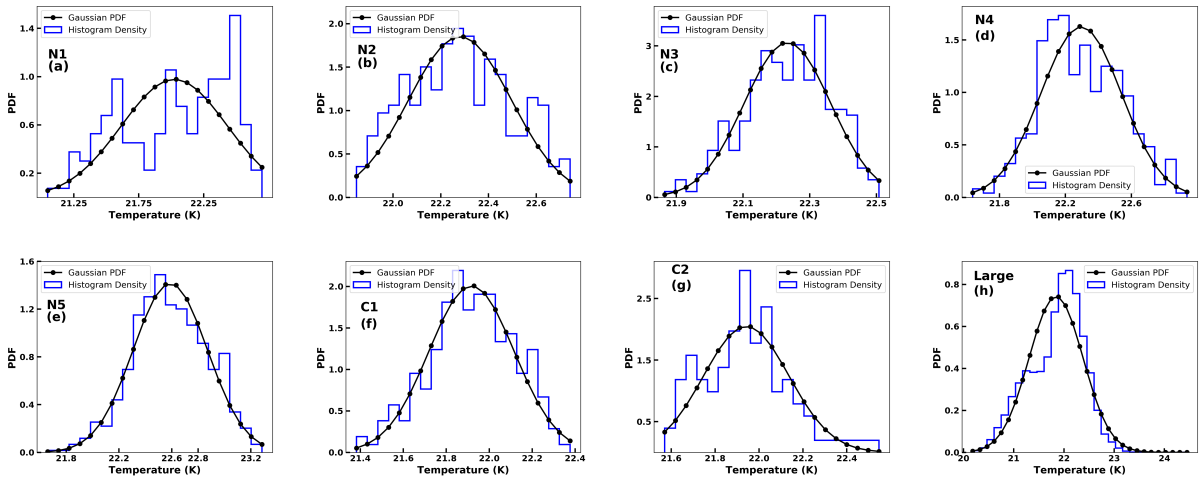

FIGURE 5. Figure shows the Gaussian distribution for dust color temperature for all sub−structures and large structure. In all figure the dust color temperature is taken along X-axis and their PDF are taken along Y-axis.

Inclination Angle

The inclination angle of the isolated region of every sub−structures is calculated by using the Holmberg (1946) formula [13] by taking the value of q* equal to 0.23 [14] for oblate spheroidal structure. The isolated region in image of 100 μm infrared flux is considered for the calculation of inclination angle. The major and minor axis of the isolated region is calculated from Aladin v2.5. The **TABLE VII** presents value of major axis (a), minor axis (b), position angle (PA) for major and minor axis and inclination angle (i). In all sub−structures the inclination angle $i > 45^\circ$ representing the *edge−on* in shape.

TABLE VII. Inclination angle of all sub−structures is shown in table.

	a (arcmin)	b (arcmin)	PA Major (deg)	PA Minor (deg)	i (deg)
N1	30.33	8.81	351.0	238.0	79.54
N2	35.34	13.8	91.9	188.1	71.12
N3	34.95	16.78	305.9	244.7	64.35
N4	42.07	22.43	173.1	283.4	64.41
N5	88.20	15.1	138.0	69.8	90.00
C1	29.81	17.42	53.5	141.4	56.52
C2	21.47	13.39	225.0	270.8	53.47

CONCLUSIONS

Following are the major conclusions of this research work:

- The dust color temperature of all the nebulae and cavities are lies between the 20 K to 24 K, with range not more than 3 K, suggesting that all the sub−structures are moving towards the thermal stability.
- The dust mass also reports the similar mass composition within all sub−structures.
- A good linear fit is observed between the infrared flux at 60 μm and 100 μm wavelength.
- The study of contour plot shows the nonuniform variation of dust color temperature and dust mass among all sub−structures, this might be due to the effect of background objects embedded within dust cloud.
- The inclination angle of shows the all sub−structures are *edge−on* in shape.
- Study of Gaussian distribution of dust color temperature shows the sub−structures are more or less disturbed by the background sources observed in the SIMBAD database, which includes the various type of stars and ISM components.

ACKNOWLEDGMENTS

This research work is done under the University Grants Commission, Small Research Development and Innovation Grants 077/078, award no.: SRDIG−77/78−S&T−5. Author want to acknowledge UGC for providing the grants in this research work and his host institution, Department of Physics, Tri−Chandra Multiple Campus, TU for all kinds of support. Thanks to the SkyView Virtual Observatory, SIMBAD and Gaia for the data used in this research work.

REFERENCES

1. A. Thapa, M. Paudel, and B. Pant, Journal of Nepal Physical Society **5**, 74–84 (2019).
2. A. Jha and B. Aryal, BIBECHANA **15**, 70–78 (2018).
3. A. Jha and B. Aryal, J. Astrophys. Astron. **39**, 1–7 (2018).
4. A. Jha and B. Aryal, Journal of Nepal Physical Society **4**, 33–41 (2017).
5. M. Paudel, P. Bhandari, and S. Bhattarai, Journal of Nepal Physical Society **7**, 110–118 (2021).
6. M. Paudel and S. Bhattarai, Journal of Nepal Physical Society **7**, 59–66 (2021).
7. M.-A. Miville-Deschênes and G. Lagache, Astrophys. J. Supp. Ser. **157**, 302 (2005).
8. D. O. Wood, P. C. Myers, and D. A. Daugherty, Astrophys. J. Supp. Ser. **95**, 457–501 (1994).
9. S. L. Schnee, N. A. Ridge, A. A. Goodman, and J. G. Li, Astrophys. J. **634**, 442 (2005).
10. X. Dupac, J.-P. Bernard, N. Boudet, M. Giard, J.-M. Lamarre, C. Mény, F. Pajot, I. Ristorcelli, G. Serra, B. Stepnik, *et al.*, Astron. Astrophys. **404**, L11–L15 (2003).
11. K. Young, T. Phillips, and G. Knapp, Astrophys. J. **409**, 725–738 (1993).
12. R. H. Hildebrand, Quar. J. R. Astron. Soc. **24**, 267 (1983).
13. E. Holmberg, Medd. Lund Astron. Obs. Ser. II **117**, 3–82 (1946).
14. M. P. Haynes and R. Giovanelli, Astron. J. **89**, 758–800 (1984).
15. F. Bonnarel, P. Fernique, O. Bienaymé, D. Egret, F. Genova, M. Louys, F. Ochsenbein, M. Wenger, and J. G. Bartlett, Astron. Astrophys. Supp. Ser. **143**, 33–40 (2000).
16. A. G. Brown, A. Vallenari, T. Prusti, J. De Bruijne, C. Babusiaux, M. Biermann, O. Creevey, D. Evans, L. Eyer, A. Hutton, *et al.*, Astronomy & Astrophysics **649**, A1 (2021).